NANO · MICRO small
www.small-journal.com

Smart Hydrogel Microfluidics for Single-Cell Multiplexed Secretomic Analysis with High Sensitivity

*Myat Noe Hsu, Shih-Chung Wei, Song Guo, Dinh-Tuan Phan, Yong Zhang, and Chia-Hung Chen**

Secreted proteins determine a range of cellular functionalities correlated with human health and disease progression. Because of cell heterogeneity, it is essential to measure low abundant protein secretions from individual cells to determine single-cell activities. In this study, an integrated platform consisting of smart hydrogel immunosensors for the sensitive detection of single-cell secretions is developed. A single cell and smart hydrogel microparticles are encapsulated within a droplet. After incubation, target secreted proteins from the cell are captured in the smart hydrogel particle for immunoassay. The temperature-induced volume phase transition of the hydrogel biosensor allows the concentration of analytes within the gel matrix to increase, enabling high-sensitivity measurements. Distinct heterogeneity for live cell secretions is determined from 6000 cells within 1 h. This method is tested for low abundant essential secretions, such as interleukin-6, interleukin-8, and monocyte chemoattractant protein-1 secretions of both suspended cells (HL60) and adherent cells (MCF7 and MDA-MB-231). This platform is highly flexible and can be used to simultaneously measure a wide range of clinically relevant cellular secretions; it thus represents a novel tool for precise biological assays.

1. Introduction

Secreted proteins such as cytokines and growth factors are essential regulators of cellular behavior correlated with immunological functions, tumour progression, and stem cell programming.[1] It has been observed that even a genetically identical cell population shows distinct phenotypic behaviour due to cellular heterogeneity, particularly in secretions, in response to environmental stimulations.[2] However, difficulty in assessing the secretion heterogeneity has been emerging as a significant barrier in monitoring disease progression, cellular pharmacological responses, and drug resistance. Nevertheless, single cell secretomic analysis is necessary for obtaining important biological information, thus requiring systematic investigations.

At present, two main methods are used to measure single-cell proteins: flow cytometry-based approaches and microwell-based immunoassay approaches. Flow cytometry represents a promising tool for effective single-cell screening by labelling cell surface biomarkers through antibodies and can be extended to determine a range of single-cell activities with a high throughput ($\approx 10^3$ s^{-1}), thus enabling us to rapidly screen a large number of cells ($\approx 10^5$–10^6 cells).[3] This platform was further developed to determine intracellular proteins within the cytoplasm.[3,4] However, challenges remain in directly measuring secreted proteins. Quantification of intracellular proteins has not been able to adequately represent secreted protein profiles. Moreover, intracellular staining requires cell fixing,[5] causing cell death after screening.

Microwell-based immunoassay approaches were developed for single-cell secretomic analysis. For example, several cells were allocated into a well-designed microtiter plate (ELISpot assay) that has been coated with a layer of primary antibody for secretion analysis.[6] After incubation, the secreted proteins from single cells were attached to the antibodies located proximal to the cells in the microwells, showing fluorescence signals representing single-cell secretions. This platform was further developed to determine multiple types of secretions by using fluorescent dyes to express signals with different wavelengths.[7] Recently, effective single-cell multiplexing secretions were measured by allocating single cells in a subnanoliter microchamber array integrated with high-density antibody barcodes for the simultaneous detection of multiple cytokines from a cell in a parallel array.[8,9] This platform was used to measure a range of multiple secretions of human cell lines and primary cell samples dissociated from the fresh tumors of patients to assess their distinct heterogeneity. Despite its advantages, the

M. N. Hsu, Prof. Y. Zhang, Dr. C.-H. Chen
NUS Graduate School for Integrative Sciences and Engineering
National University of Singapore
Singapore 117456, Singapore
E-mail: biecch@nus.edu.sg
M. N. Hsu, Dr. S.-C. Wei, Dr. S. Guo, Dr. D.-T. Phan, Prof. Y. Zhang, Dr. C.-H. Chen
Department of Biomedical Engineering
National University of Singapore
Singapore 117574, Singapore
M. N. Hsu, Dr. S.-C. Wei, Dr. C.-H. Chen
Biomedical Institute for Global Health Research and Technology (BIGHEART)
Singapore 117599, Singapore
Dr. C.-H. Chen
Singapore Institute for Neurotechnology (SINAPSE)
Singapore 117456, Singapore
The ORCID identification number(s) for the author(s) of this article can be found under https://doi.org/10.1002/smll.201802918.

DOI: 10.1002/smll.201802918

cell throughput of these platforms is limited by the number of microwells in a microtiter plate.[1]

Recently, droplet microfluidics has emerged as an important technology which has provided new experimental possibilities for single-cell screening with high efficiency. A large amount of cell-containing monodispersed droplets can be produced continuously, thus enabling the effective compartmentalization of single cells for assaying.[10] This platform was developed to measure single-cell secretions by encapsulating single cells and customized chemical sensors. For example, cell-secreted enzyme activities have been investigated by conducting fluorescence resonance energy transfer (FRET)-based sensors within droplets for biological sample profiling and diagnosis in a high throughput manner.[11] However, most of the droplet-based approaches only largely focused on metabolomic or FRET-based detections since heterogeneous immunoassays that require washing steps are not well suited to the droplet format.[11–14] Although immunoassay format in droplets has been demonstrated using magnetic relocation approaches for immunoglobulin G (IgG)-secreting cells,[15] it suffers from high fluorescence background due to the absence of washing steps, resulting in low sensitivity. This limitation could be addressed by utilizing agarose droplets impregnated with polystyrene capture beads, hence allowing the subsequent washing of the cross-linked hydrogel particles.[16] However, this method was employed to study the stimulated Jurkat T cells with high secretion activities, reaching the limitation to measure low abundant important secretions from single cells without stimulations.

In this study, we introduced an integrated single-cell secretomic analysis platform to determine multiple secreted proteins from single cells with high sensitivity. Novel smart hydrogel particles were synthesized as the sensors for secreted proteins by modifying poly (*N*-isopropylacrylamide) (PNIPAM) with acrylic acid to conjugate multiple antibodies. The temperature-induced shrinkage of the PNIPAM hydrogel particles allowed the concentration of analytes within the gel matrix to increase fivefold, enabling instant signal amplification (within 10 s) with enhanced sensitivity (≈30 pM). The combination of droplet-based single cell encapsulation and smart hydrogel-based immunoassay was synergistic. Individual cells were effectively isolated with each microgel immunosensors while enabling sensitive multiplexed detection of the accumulated secretions for effective biological sample profiling (Table S1, Supporting Information). We demonstrated the utility of this device for determining multiple secretions such as interleukin-6 (IL-6), interleukin-8 (IL-8), and monocyte chemoattractant protein-1 (MCP-1) from both suspended leukemia cells and adherent breast cancer cells to assess the distinct cellular heterogeneity between single-cell secretomic signatures. This technology builds upon prior successes in single-cell encapsulation in droplets as well as antibody-based immunoassays while utilizing simplified schemes of sample handling and analysis. Using smart hydrogel sensors with high sensitivity to measure important and low-abundance secreted proteins resulted in a novel multiplexed single-cell secretomic assay, which can be applied to a range of advanced biological analysis purposes and physiological sample profiling.

2. Results and Discussion

2.1. Smart Hydrogel Microfluidic Approach

To detect protein secretions at the single-cell level, individual cells were coencapsulated into 700 pL (≈110 µm) droplets with a poly (*N*-isopropylacrylamide-*co*-acrylic acid) P(NIPAM-*co*-AAc) functional hydrogel particle (35 µm) as an immunosensor functionalized with specific antibodies for IL-6, IL-8, and MCP-1 (**Figure 1**a). These droplets were incubated at 37 °C for 24 h to allow the accumulation of single cellular secretome. The analytes also became bound to the functionalized hydrogel particles during the incubation period. Afterward, the hydrogel particles were retrieved, washed, and probed with detector antibodies, which were each conjugated with a specific fluorophore. Then, by increasing the temperature above the lower critical solution temperature (LCST) of ≈38.5 °C, the shrinking of hydrogel particles was induced to enhance the fluorescence by approximately fivefold, thus allowing the detection of low-abundance secretome from single cells (Figure 1b).

Monodispersed hydrogel microbeads were fabricated using a cross-junction droplet generation device (Figure S1, Supporting Information) prior to their functionalization with capture primary antibodies (IgGs). Covalent coupling enables the stable immobilization of the capture antibodies without the leaching problems typically associated with physical absorption approaches.[17] For PNIPAM-based gels, additional functional groups are required to perform covalent modifications. Hence, carboxylic acid groups were incorporated by copolymerizing with acrylic acid (AAc), yielding *P*(NIPAM-*co*-AAc) hydrogel particles. Fourier transform infrared spectroscopy (FTIR) was carried out to analyze the chemical compositions and structures of the prepared microspheres (**Figure 2**a). In addition to the characteristic amide I (1650 cm^{-1}) and amide II (1540 cm^{-1}) bands[18] of PNIPAM, a band at 1720 cm^{-1}, which represents the stretching vibration of carboxylate acid groups,[19] was observed in the FTIR spectra of the *P*(NIPAM-*co*-AAc) samples, indicating successful copolymerization products. Upon functionalizing the hydrogel particles with capture IgGs, the band at 1720 cm^{-1} diminished as the −COOH groups were converted to form amide linkages. At the same time, the amide I band (1650 cm^{-1}) and amide III (1220 cm^{-1})[20] region became more prominent due to the covalent coupling to antibodies. In addition, the appearance of a 1060 cm^{-1} band corresponding to the polysaccharides could be attributed to the glycosylated state of the immobilized IgGs,[20] thus confirming the presence of capture IgGs on the gel matrix.

The robust target capture by immobilized antibodies should be ensured for optimized assay sensitivity. The 3D nature and increased effective surface area of hydrogel particles allowed for a higher capture probe density than conventional surface-based assay formats. The hydrated and nonrigid gel matrix also improved the target binding kinetics by reducing steric issues,[21,22] potentially augmenting assay performances. However, more often than not, hydrogel-based systems suffer from diffusion limitations,[17,23,24] giving rise to large assay variabilities and reduced detection capabilities. Therefore, an interconnected pore structure with significantly large pores is crucial for allowing target proteins to diffuse freely through

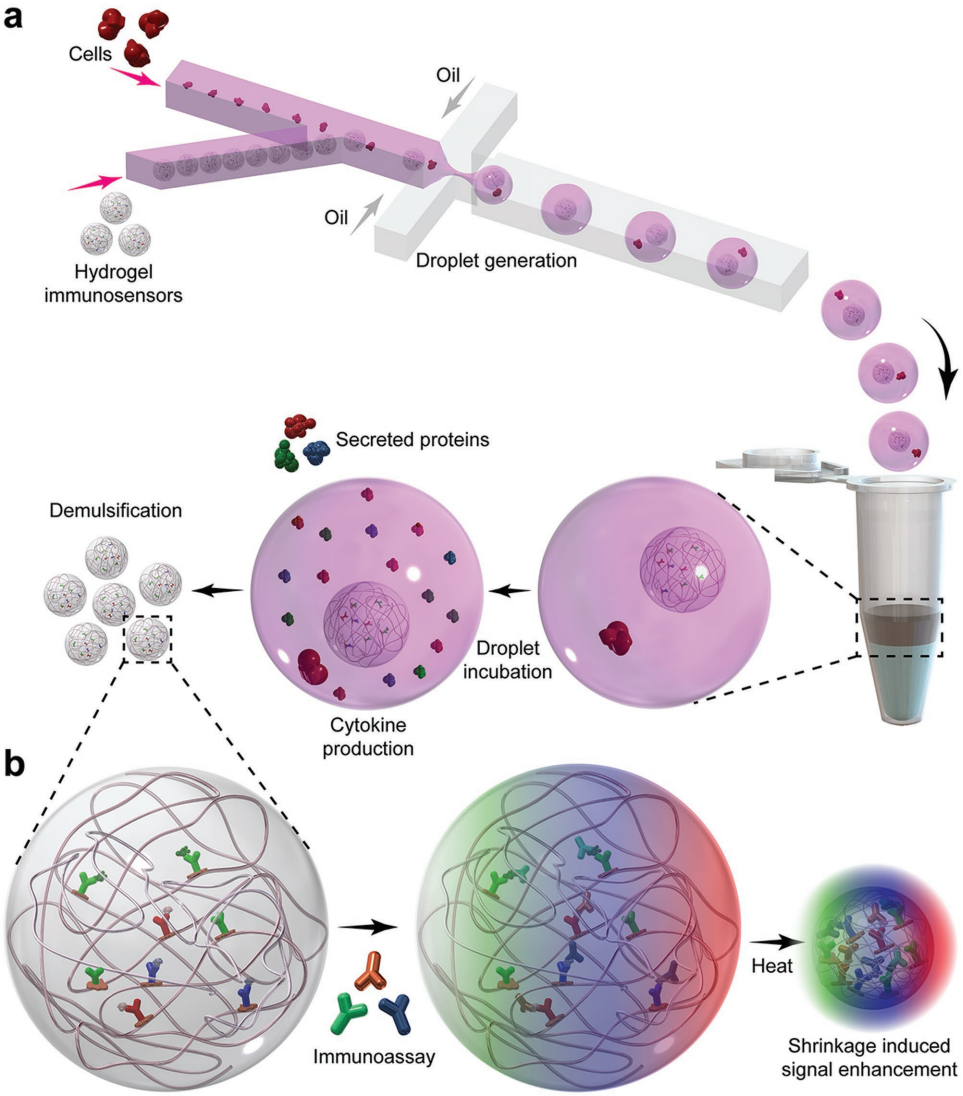

Figure 1. A platform for the sensitive detection of single cellular protein secretion: a) Cells were coencapsulated with hydrogel particle immunosensors in a droplet. The droplets were incubated for 24 h to allow cytokine secretions from the cells to be captured and concentrated on the hydrogel particle. The hydrogel particles were then retrieved and immunoassay was carried out for the quantification of secreted analytes. b) Immunoassay with further sensitivity enhancement was achieved by temperature-induced shrinkage of thermoresponsive P(NIPAM-*co*-AAc) immunosensors.

P(NIPAM-*co*-AAc) gels. A range of porosities was explored by adding inert poly (ethylene glycol) (PEG) as a porogen during the fabrication process. The polymerization-induced phase separation of nonreactive PEG[25] from the growing *P*(NIPAM-*co*-AAc) chains resulted in a larger mesh structure that could be controlled by the porogen's molecular weight. As shown in the scanning electron microscopy (SEM) images in Figure 2b, greater pore-size enhancements were achieved with higher PEG molecular weights. However, the structural integrity of the hydrogel particles was affected when PEG 35 000 was used, which often resulted in weak, broken, or polydisperse gel particles. On the other hand, the PEG 6000 porogen yielded interconnected macroporous structures, while remaining structurally stable throughout the multiple rounds of rigorous washing steps required in the immunoassay process.

The capture probe density was optimized. The extent of antibody conjugation was fine tuned by controlling the amount of carboxylic acid moiety. As illustrated in Figure 2c, by increasing the AAc copolymer ratio, a higher immobilization density of fluorescent antigoat antibodies could be achieved in the hydrogel particles. However, at a high probe density, the capture antibodies were packed in close proximity, leading to the reduced target accessibility to those probes.[26] Furthermore, previous studies have established that a higher hydrophilic AAc content (>5%) has the tendency to form predominantly microporous or mesoporous structures[27] despite the presence of the PEG porogen. Additionally, as analytes were captured on the probes, the effective pore size was further reduced, thus preventing other target molecules from reaching the inner probes. This probe inaccessibility phenomenon is shown in Figure 2d, where the fluorescence goat IgG target was unable to reach the centre

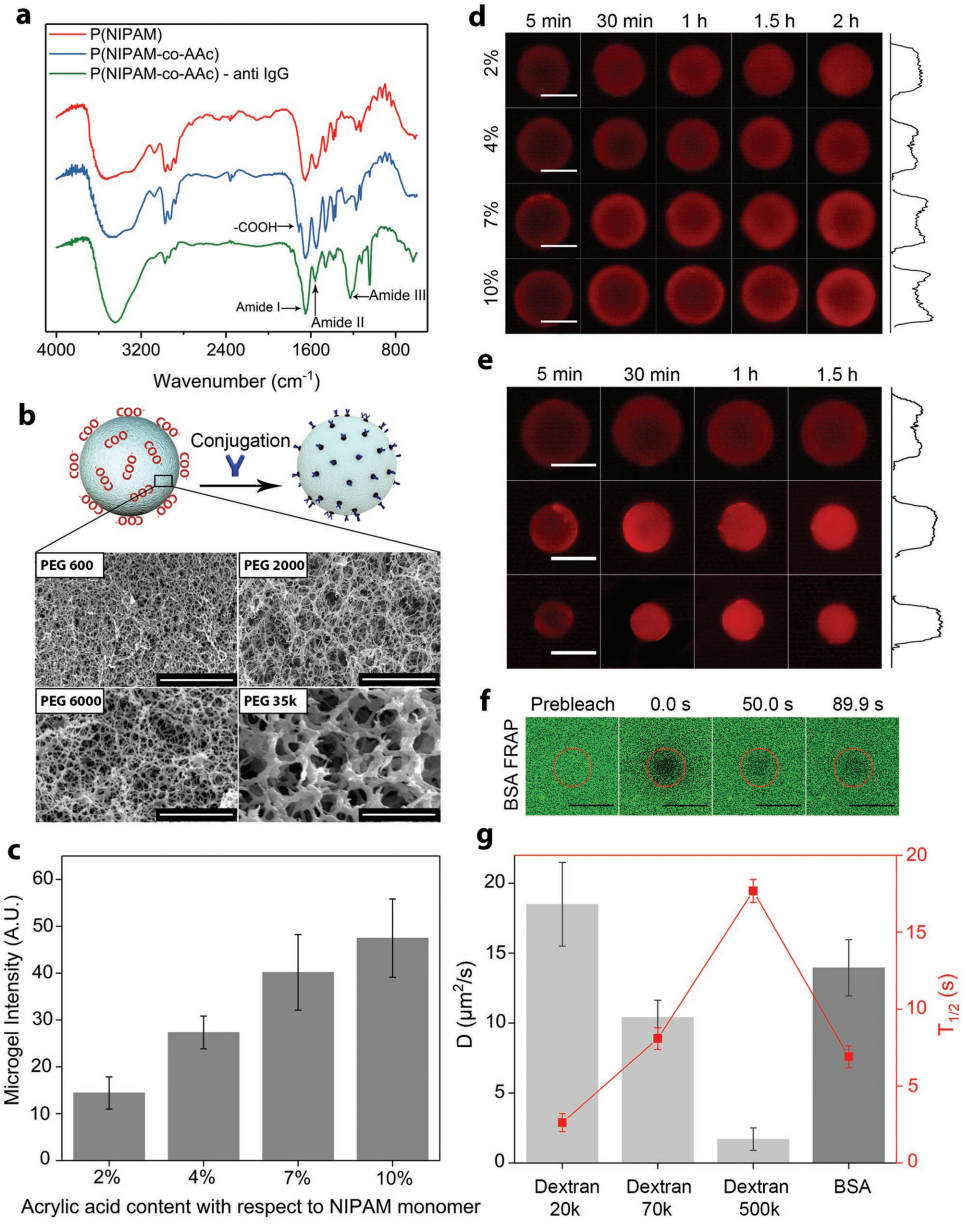

Figure 2. Characterization of P(NIPAM-*co*-AAc) hydrogel particles: a) FTIR spectrum showing successful incorporation of −COOH groups as well as successful utilization of the −COOH groups to immobilize capture antibodies. b) SEM images showing interconnected pore structures of the prepared hydrogels. Each scale bar represents 3 µm. c) The intensity of hydrogel particles resulting from immobilized anti-goat-Alexa350 antibodies. The error bars represent the standard deviation for each sample group ($n = 20$). d) Diffusion of goat IgG-Alexa568 into hydrogel particles of different acrylic acid contents e) and different sizes. Each scale bar represents 40 µm. f) Different phases of FRAP experiment for FITC–BSA diffusion in P(NIPAM-co-AAc). Each scale bar represents 5 µm. g) Calculated $T_{1/2}$ and D values of FITC-Dextran of different molecular weights and FITC-BSA in P(NIPAM-co-AAc). The error bars represent the standard deviation for each sample group ($n = 3$).

of the microparticles, especially for hydrogel particles with AAc contents of 7% and 10%. The intensity profile plots revealed that the target protein was confined near the outer rim of the gel particles, even with relatively long incubation duration of 2 h. Obviously, a balance between probe density and accessibility is required to achieve an optimum assay condition. As such, the size of the hydrogel particles was reduced to shorten the diffusion path length while maintaining a moderate AAc content of 4%. The reduction in hydrogel particle diameter was achieved by simply increasing the oil flow rate during the prepolymer droplet generation step (Figure S1, Supporting Information). For smaller microparticles, uniform intensity profiles were obtained within 1 h (Figure 2e), illustrating the diffusibility of analytes throughout the particles and their easy accessibility to the innermost probes.

To assess the target penetration abilities in the 4% AAc hydrogel particles with PEG 6000 as the porogen, the fluorescence recovery after photobleaching (FRAP) experiments

(Figure 2f,g) was assessed using different molecular weights of fluorescein isothiocyanate-dextran (FTIC-dextran). Half-recovery times ($T_{1/2}$) and diffusion coefficients (D) were calculated following the methods reported by Jönsson et al.[28] $T_{1/2}$ increased and D decreased with the increasing molecular weight of the diffusing molecule. In fact, diffusion became significantly limited for larger molecules at 500 kDa. Indeed, most secreted proteins and detector antibodies have relatively smaller molecular weights, which do not exceed ≈150 kDa. Overall, for 35 µm hydrogel particles, smaller proteins, such as secreted cytokines, have a short penetration time (T_p) of ≈17 s, while larger antibodies require a longer penetration time of 29 s $< T_p <$ 180 s (Table S2, Supporting Information). A representative protein, bovine serum albumin (FITC-BSA) (67 kDa), was observed to have similar diffusion characteristics as 70 kDa FITC-dextran and required 22 s for penetration. Hydrogel networks with similar characteristics typically require an incubation duration of 30 min to fully penetrate the gel network.[22,29] However, in this study, an incubation time of 1.5 h was employed to ensure that the binding equilibrium was fully reached.

2.2. Sensitivity Enhancement of Hydrogel Immunosensor

The advantage of the *P*(NIPAM-*co*-AAc) immunosensor is its inherent ability to concentrate the binding signal from the immunocomplexes that it carries. Due to its isopropylamine pendant groups, PNIPAM-based hydrogels undergo a volume phase transition from a swollen hydrated state to a shrunken dehydrated state when heated beyond their LCST at ≈32 °C.[30] Hydrophobic chain interactions become dominant as the hydrogen bond interactions weaken above the LCST, leading to the removal of water molecules from the matrix and the subsequent collapse of the polymer chain.[30,31] As a result, the hydrogel microparticles appear to shrink when heated, allowing the signal to concentrate in a smaller region. The temperature response behavior of *P*(NIPAM-*co*-AAc) was characterized by tracking the changes in hydrogel particle size across various temperatures. LCST was defined as the temperature at which the hydrogel particles reached 50% of their initial sizes. At a pH of 7.2, the presence of hydrophilic copolymer AAc increased the LCST to ≈38.5 °C (Figure S2, Supporting Information). As the hydrogel particles were heated above the LCST, their fluorescence intensities increased in a similar manner as the shrinkage response curve (**Figure 3**a). Interestingly, the reduction in hydrogel particle diameter was linearly correlated to the enhancement in signal intensity (Figure 3b), granting the users additional control for signal amplification. Most importantly, the temperature-induced shrinkage was isotropic, and the response time was remarkably short (<10 s). Therefore, well-defined fluorescence signal amplification could be achieved almost instantly without the need for conventional enzymatic reactions. This enabled the improvement of assay sensitivities and detection limits while minimizing the assay complexities and possible sources of contamination.

The detection capability of the immunosensors was examined by generating the standard calibration curves for each target (Figure 3c–e). Protein analytes were spiked into cell culture media after a blocking step to minimize nonspecific signals. Conservative incubation times were also employed to approach optimum limits of detection (LOD) and signal-to-noise ratios. LODs, intrarun coefficients of variation (CVs), and detection sensitivities were assessed from the standard calibration curves (**Table 1**). Sensitivity values were obtained from the slope of each standard curve. LOD was defined as the concentration where the average background-corrected signal divided by the standard deviation of the blank sample was equal to 3. The dynamic linear ranges of the assay for each analyte were also summarized in Table 1. Overall, the temperature-driven signal concentration step at 50 °C improved both LODs and detection sensitivities. Reasonably low standard deviations were also obtained throughout the linear dynamic range for each assay, yielding CVs (<15%) that were tolerable by laboratory standards.[32] Low CV values were essential for single-cell measurements, so that the variations observed could be attributed to cellular heterogeneity. In this platform, the CVs were comparable to those of other reported single-cell assays such as intracellular staining and ELISpot.[33–35] Slight variations observed across the microparticles could be attributed to the uneven immobilizations of multiple capture probes in an Intraplex format where all three capture antibodies were conjugated on a single hydrogel particle (Figure 3f) with the help of the F_c binding protein A. Improvements in CVs could be achieved by ensuring excess capture probe and continuous mixing during the immobilization step. In addition, the microgels could be heated in a microfluidic observation chamber to allow even heat flow for homogeneous signal enhancement process.

Determining the cross reactivity of antibodies is one of the major challenges in multiplexing assays, despite the emergence of validated antibody pairs. To achieve the simultaneous detection of the three cytokines, it is vital to assess the specificity of the antibody pairs. Hence, all possible combinations of the three targets were examined to identify any potential sources of false signals (**Table 2**). In addition, the recovery values of the culture media spiked-in cytokines were calculated as a percentage of the actual concentration used. Notably, no significant sources of cross reactions were detected, and the recovery values of the spiked-in samples fell within 15% of the values calculated from the standard calibration curves.

2.3. Single-Cell Secretomic Analysis

To measure single cellular secreted proteins, *P*(NIPAM-*co*-AAc) immunosensors were coencapsulated with the cells into droplets. The coencapsulation device consisted of three inlets for 1) hydrogel particle immunosensors, 2) cell suspension, and 3) carrier oil. The device had two junctions: the microparticles were delivered into the cell coflow at the first junction and coencapsulation into droplets occurred at the second junction (Figure S3, Supporting Information). This fluidic chip could generate 500–1000 pL droplets at a rate of ≈80–140 droplets per second depending on the flow conditions employed. To ensure the smooth flow of the deformable microbeads, the microfluidic channels were treated sequentially with 1% silane and 1% poly vinyl alcohol prior to the operation of the device (Figure S4, Supporting Information). The hydrogel particles were then closely

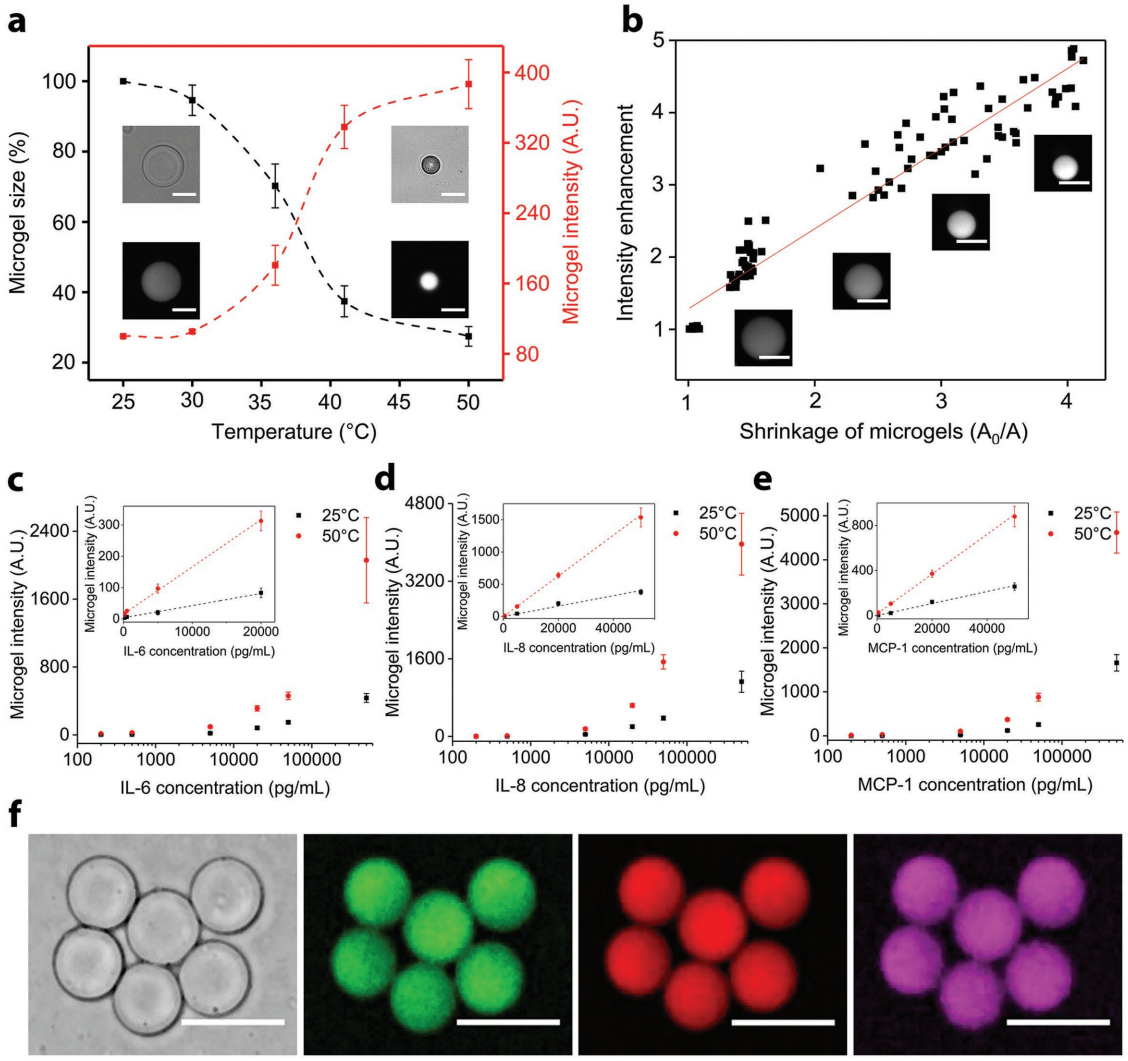

Figure 3. Characterization of hydrogel particle immunosensors with signal enhancement. All error bars represent the standard deviation for each sample group (n = 20): a) Temperature-dependent intensity enhancement of hydrogel particles. Each scale bar represents 25 µm. b) Correlation between intensity enhancement and changes in the cross-sectional area of hydrogel particles. Each scale bar represents 25 µm. c–e) Standard calibration curves for the detection of c) IL-6, d) IL-8, and e) MCP-1 at 25 and 50 °C. Insets show the linear range of the standard curves. f) Intraplex signal of hydrogel particle immunosensors (green: IL-6, red: IL-8, and purple: MCP-1). Each scale bar represents 50 µm.

packed at the side channel to allow regular release, thereby enabling a hydrogel particle encapsulation efficiency of nearly 90%.[36–39] As a result, almost all cells were paired with hydrogel particles. There was also no cell size bias for encapsulation since the channel dimensions were relatively large. Furthermore, since cell encapsulation is a random process that follows a Poisson distribution,[16] cell solutions were diluted and passed through a 40 µm strainer to minimize multiple-cell droplet events. The rate of multiple-cell encapsulations depended on the initial cell density used and generally fell within the acceptable range of ≈5% (**Figure 4**a,b). However, the main challenge comprised ensuring that each cell was paired with one hydrogel particle since the droplets containing at least one cell and one hydrogel particle would result in a positive binding signal. Among these positive droplets, over 80% of the droplets were observed to contain exactly one cell and one hydrogel particle (inset, Figure 4a,b). Nevertheless, the presence of multiple-cell events (≈10% of all positive signals) did not obscure rare cellular behaviors,[16,37] as the majority of rare events were still found as singlets.

The next important requirement of the platform is that the cells must be in an active state in the droplets. Therefore, we

Table 1. LODs, CVs, sensitivities and linear detection ranges for hydrogel particle immunoassays in Intraplex format.

	LOD [pM]	CV [%]	Sensitivity	Range [$\log_{10}$]
IL-6 (25 °C)	96.4	26.8	0.004	1.6
IL-6 (50 °C)	34.6	14.6	0.02	
IL-8 (25 °C)	46.0	23.1	0.008	2
IL-8 (50 °C)	25.0	14.4	0.03	
MCP-1 (25 °C)	55.9	20.6	0.005	2
MCP-1 (50 °C)	30.8	11.9	0.02	

Table 2. Intraplex detection of the three cytokines reported as (average signal ± standard deviation). The absence of target (–) corresponds to a negative signal, while the presence of target (+) correctly corresponds to a positive signal. Average hydrogel particle fluorescence signals were obtained after temperature-induced shrinkage (n = 20). IL-6 was spiked at 20 ng mL^{-1}. IL-8 and MCP-1 were spiked at 40 ng mL^{-1}.

Target			Hydrogel particle fluorescence (A.U.)		
IL-6	IL-8	MCP-1	IL-6	IL-8	MCP-1
–	–	–	21.2 ± 5.3	15.5 ± 5.1	4.8 ± 0.8
–	–	+	6.5 ± 3.8	19.2 ± 4.1	714.1 ± 29.0
–	+	–	26.2 ± 6.4	1256.1 ± 138.1	10.0 ± 4.8
+	–	–	308.3 ± 32.7	25.0 ± 3.5	13.2 ± 7.1
–	+	+	31.7 ± 6.5	1316.1 ± 151.0	699.9 ± 51.1
+	–	+	370.7 ± 42.1	13.1 ± 3.5	826.0 ± 105.0
+	+	–	344.1 ± 55.6	1153.2 ± 102.1	20.4 ± 6.3
+	+	+	345.1 ± 16.0	932.0 ± 84.0	972.0 ± 133.0
Recovery (%)			108.2 ± 7.1	92.2 ± 9.4	111.5 ± 9.0

examined the cellular viability in picoliter droplets for up to 72 h. The cell viability in droplets remained high (at >90%) after 24 h (Figure 4c). Afterward, the viability dropped drastically, possibly due to the lack of nutrient availability and waste by-product removal. As such, a 24-h incubation period was employed for the accumulation of cellular secretions within droplets. To investigate the cytokine production ability of the suspended cells in droplets, particularly for the naturally adherent cells, enzyme-linked immunosorbent assay (ELISA) experiments were performed for both the adhered and suspended cultures of all cells. The ELISA results showed great agreement between the two culture types (Figure S5, Supporting Information), demonstrating the biologically active state of the cells. This result shows that the droplet environment is suitable for the analysis of the single cellular secretion products of 24 h for both adhered and suspended cells.

Single cellular overnight cytokine secretion profiles were studied using both suspended cells (HL60 acute promyelocytic leukaemia cells) and adherent cells (MCF7 and MDA-MB-231 breast cancer cells). A positive secretion signal was defined as a background-corrected hydrogel particle signal that was three times higher than the standard deviation of a negative sample. In this study, the analysis of more than 15 000 gel beads resulted in an average of 1000 positive secretion signals per cell type. However, the cell throughput could be easily scaled up by adjusting the droplet collection time. Using our platform, 10^6 droplets, out of which 10^5 droplets contained single cell, could be generated in ≈1 h.

In accordance with bulk ELISA experiments (Figure S6, Supporting Information), HL60 cells were observed to secrete predominantly IL-8 and MCP-1, while MDA-MB-231 secreted all three cytokines. Similarly, MCF7 showed almost no secretions (**Figure 5**a). The in-droplet conditioning of the cells with 50 ng mL^{-1} tumor necrosis factor alpha (TNFα), which is a well-known cytokine linked with tumor progression,[39,40] elevated the single cellular secretion of the three cytokines, except for MCF7 cells, which maintained their low secretion activities (Figure 5a). The increased expressions of IL-6, IL-8, and MCP-1 were also further confirmed by bulk ELISA analysis. Notably, by virtue of the simultaneous detection of multiple analytes, distinct secretion profiles were obtained for each cell type (Figure 5b,c). The signal enhancement afforded by the temperature-induced shrinkage of immunosensors at 50 °C allowed for the analysis of secretion levels, and hence secretomic heterogeneity, at a better resolution. Interestingly, an aggressive and invasive cell line, MDA-MB-231, exhibited the highest secretion levels with the greatest degree of heterogeneity. Upon

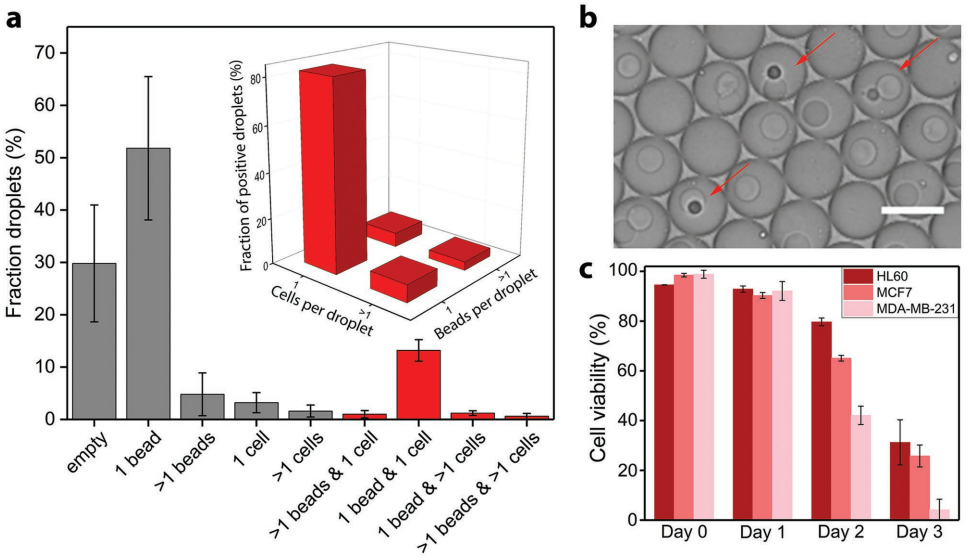

Figure 4. Single-cell secretion assay characterization: a) Cell and hydrogel particle coencapsulation statistics across three independent experimental runs. The inset shows a high 1:1 cell: hydrogel particle pairing among droplets with positive signals. The error bars represent standard deviation from three different independent experimental runs. b) Bright field image showing cell and hydrogel particle coencapsulation in the droplets. The red arrows indicate the desired droplets with exactly one cell and one hydrogel particle. The scale bar represents 100 µm. c) Cell viability in droplets. The error bars represent the standard deviation for each sample group (n = 50).

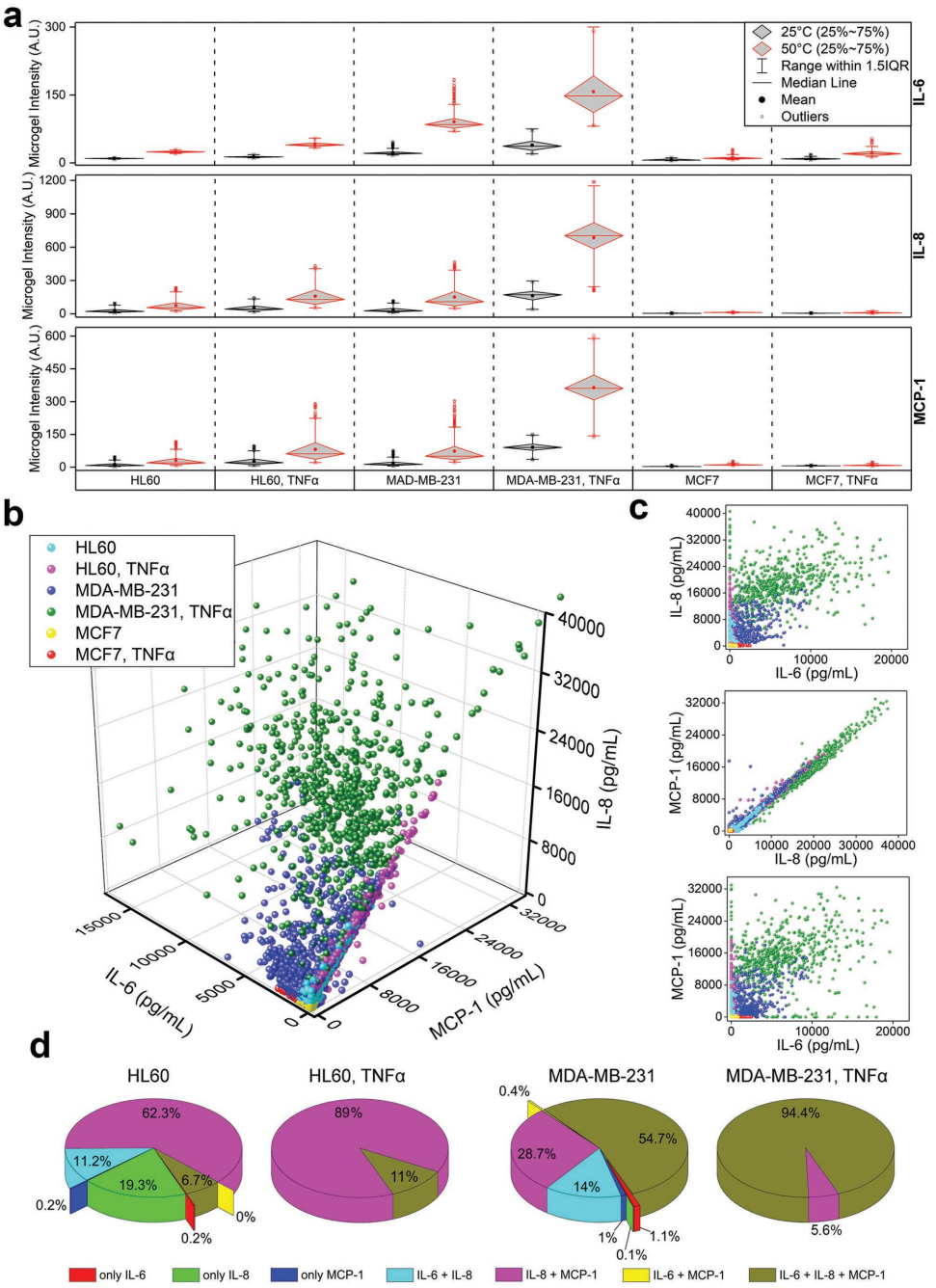

Figure 5. Single-cell secretion from at least 1000 cells from each cell line: a) Hydrogel particle intensities corresponding to measurements at 25 and 50 °C for various cytokines show an enhanced ability to detect cellular heterogeneity. Lower and upper ✖ values represent the 1st and 99th percentiles of the data, respectively. b) Single cellular cytokine secretion profile for various cell lines in a 3D scatter plot and c) 2D scatter plots. d) Secretion heterogeneity present in the types of cytokines produced by individual cells.

activation with TNFα, MDA-MB-231 showed even greater heterogeneity. HL60 cells showed similar trends, where the IL-8 and MCP-1 secretion levels were enhanced after being spiked with TNFα. However, the increase was not as noticeable as that of MDA-MB-231.

Further analysis revealed the existence of subpopulations that secreted distinct sets of target cytokines. A total of 19.3% of HL60 cells mainly secreted IL-8 only. The majority (62.3%) secreted both IL-8 and MCP-1, while a small population (6.7%) secreted all three cytokines. Interestingly, the HL60 population became less diverse upon TNFα activation, as the cells secreted more cytokines. For instance, the preactivation subpopulations that secreted only one of the tested cytokines no longer existed postactivation. The majority of TNFα-spiked HL60 secreted IL-8 and MCP-1, while 11% secreted all three proteins. Similar secretion trends were also observed for MDA-MB-231. Prior to

TNFα conditioning, diverse subpopulations were discovered, with most of the cells (97.8%) producing at least two of the analytes. Among them, 54.7% secreted all the tested cytokines. Much smaller subpopulations that released only one of the cytokines were also found. However, with TNFα activation, only two distinct subpopulations that either produced all three targets or only IL-8 and MCP-1 remained.

Typically, these individual responses cannot be observed using bulk analysis. However, with the single-cell platform, the increased cytokine secretions detected in bulk ELISA could be attributed to two compounding factors, namely, 1) enhanced production at the single cellular level and 2) adjustments in cellular subpopulations that allowed the majority of cells to secrete more cytokine types.

3. Conclusion

At present, genomic analysis is the main method used for the characterization of biological samples. With amplification approaches like polymerase chain reaction for nucleic acids, high precision single cellular genomic information can be obtained relatively with ease to study a wide range of biological phenomena. However, without comprehensive single-cell secretomic analysis, genome-based detection provides an incomplete understanding of cellular activities and disease states. To address this challenge, several fluidic devices were investigated. For example, flow cytometric analysis allows the multiplexed measurement of protein markers from single cells, but most proteins are either surface receptors or cytoplasmic proteins. Several advanced immunoassay-based platforms have been developed for single-cell multiplexed secreted protein assay, but their throughput is very much limited to screening 100–1000 cells per experimental run, thus limiting their ability to screen large numbers of cells to achieve complete physiological sample profiling. Although the droplet-based single-cell secretomic analysis was previously demonstrated, they suffer from high background signals, hence limited sensitivities ($\approx\times 10^{-9}$ M). As a result, these platforms are only employed for cells with high secretion activities such as activated T-cells. Due to the lack of amplification techniques, single-cell proteomic analysis in droplets has been persistently proven to be difficult.

With the development of smart hydrogel technology, we have described a droplet-based multiplexed immunoassay chip that enables effective single-cell multiplexed secretomic analysis with high sensitivity. The novel aspect of this system is the intrinsic signal enhancement capability of the smart immunosensor. As a result, improvements in LODs and CVs were achieved while minimizing assay complexities. These traits permitted the analysis of single cellular secretion heterogeneity at a better resolution. The assay could be further improved to allow large-scale multiplexed assay by integrating with barcoding strategies of hydrogel particles, such as color, size, and shape coding. This platform thus provides significant advantages in single-cell secreted protein detection and offers complete information for biological sample profiling through large-scale screening. The secreted protein profile can complement the information offered by conventional flow cytometry. For instance, since cancer cells typically secrete a range of proteins for metastasis and migration, comprehensive analysis of cancer secretome would provide valuable information on cancer progression as well as treatment efficiency. This approach could also be used to investigate the function of immune cells such as T-cell secretions in response to specific antigens. Similarly, this platform could rapidly indicate desired target mutants according to their secretion activities to determine the quality of the mutant library generated.

In general, this platform represents a promising tool to perform single-cell secretomic analysis with high sensitivity, bringing the single-cell protein assay to a deeper level of functional analysis. A potential concern of this platform is that the cells that are suspended to be encapsulated within the droplets may experience a condition that affects the normal functioning of primary cells. Indeed, challenges remain to screen adhesive cell's secretions in their natural physiological conditions by using this approach. Another concern is that the requirement of fluorescence labels would impair the real time measurements of secretions.[41] Nerveless, our smart hydrogel microfluidic platform is a promising technology for the high-throughput analysis of protein secretion profiles from single cells and may assist in monitoring disease progression and cellular functions in patients.

4. Experimental Section

Antibody Reagents: Protein A and capture antibodies were purchased from Abcam (Cambridge, MA): natural protein A (ab7399), rabbit anti-IL-6 (ab6672), rabbit anti-IL-8 (ab7747), and rabbit anti-MCP-1 (ab9669). Reporter antibodies and protein standards were purchased from R&D Systems (Minneapolis, MN): Alexa Fluor 488-conjugated mouse anti-IL-6 (IC2061G), Alexa Fluor 594-conjugated mouse anti-IL-8 (IC208T), Alexa Fluor 647-conjugated mouse anti-MCP-1 (IC279R), recombinant IL-6 (206-IL), recombinant IL-8 (208-IL), and recombinant MCP-1 (279-MC). The ELISA kit for IL-8 (D8000C) and MCP-1 (DCP00) were purchased from R&D Systems (Minneapolis, MN). The ELISA kit for IL-6 (ab46042) was obtained from Abcam (Cambridge, MA). All secondary conjugated antibodies were from Invitrogen, CA, USA.

Cell Culture: Human breast cancer cell lines MCF7 and MDA-MB-231, as well as human promyelocytic leukaemia cell line HL60, were purchased from American Type Culture Collection (ATCC) (Manassas, VA). MCF7 and MDA-MB-231 were cultured in Dulbecco's Modified Eagle Medium (Gibco, CA, USA) supplemented with 10% heat-inactivated fetal bovine serum (FBS) (Gibco, CA, USA) and 50 μg mL^{-1} gentamicin (Gibco, CA, USA). HL60 was cultured in Iscove's Modified Dulbecco's Medium (Gibco, CA, USA) supplemented with 20% heat-inactivated FBS (Gibco, CA, USA) and 50 μg mL^{-1} gentamicin (Gibco, CA, USA). All cells were maintained at 37 °C in a 5% CO_2/95% air incubator and grown to ≈85%–90% confluency before single-cell experiments.

Hydrogel Immunosensor Synthesis: N-isopropylacrylamide (NIPAM), AAc, ammonium persulfate (APS), *N*,*N*'-methylene-*bis*(acrylamide), *N*,*N*,*N*',*N*'-tetramethylethylene-diamine (TEMED), PEG (average M_n 600, 2000, 6000, 35 000), 2-[*N*-morpholino]ethane sulfonic acid (MES), 1-ethyl-3-(3-dimethylaminopropyl)-carbodiimide (EDC), and *N*-hydroxyfulfo-succinimide (NHS) were purchased from Sigma-Aldrich (St. Louis, MO, USA). The fluorocarbon oil used was HFE-7500 (3M Novect, Singapore). Oil-based biocompatible surfactant Pico-surf 1 was purchased from Dolomite, UK.

Hydrogel particles were synthesized based on microfluidic droplet technology. The aqueous disperse phase consisted of a monomer mixture and an initiator solution, whereas the continuous phase had fluorinated HFE-7500 with 0.15% surfactant. The monomer mixture contained 20% NIPAM with various wt% AAc as a comonomer, 2%

TEMED as an accelerator, and 10% PEG as a porogen, while the initiator solution contained 1% APS. The monomer mixture and the initiator solution were brought together in the microfluidic device just before droplet creation at 1 μL min^{-1} to generate prepolymer W/O emulsions in oil. When the aqueous flow rate remained constant, varying the oil flow rate (4, 8, and 12 μL min^{-1}) yielded different droplet sizes. A free radical polymerization reaction was then allowed to take place in the droplets for 30 min. Afterward, the resulting hydrogel particles were washed and suspended in water.

The synthesized hydrogel particles were functionalized with natural protein A through EDC/NHS chemistry. In brief, hydrogel particles were incubated with 50×10^{-3} M EDC and 120×10^{-3} M NHS in 0.1 M MES coupling buffer for 30 min while being agitated at 15 rpm on a tube rotator. Afterward, the particles were washed once with phosphate buffered saline (PBS) (Gibco, CA, USA) prior to incubation with 0.5 mg mL^{-1} protein A solution for 2 h. After washing once with PBS, the resulting hydrogel particles were combined with 50 μg mL^{-1} capture antibodies in PBS for 2 h to form immunosensors. The beads were then blocked in ELISA blocking buffer (Thermo Scientific, UK) for at least an hour before usage.

FTIR: FTIR spectra were recorded to ascertain the copolymerization between AAc and NIAPM, as well as the immobilization of biological moieties on the synthesized particles. Before freeze drying, the hydrogel samples were washed with distilled water three times to remove any impurities. Thereafter, each sample was compressed into a potassium bromide pellet for FTIR measurement in the wavenumber region of 600 to 4000 cm^{-1} at a resolution of 2 cm^{-1}.

SEM: Hydrogel samples were first dehydrated through an ascending ethanol series (25%, 50%, 75%, and 90%) ending in 100% ethanol before undergoing a CO_2 critical point drying (CPD) procedure with BALTEC CPD030. The CPD-dried samples were then carefully cut to expose their internal pore structures and sputter coated with a 50 nm gold layer using BALTEC SCD005. Their porous morphologies were then examined using an FEI QUANTA 650 field emission gun SEM at an operating voltage of 10 kV.

Temperature Response Characterization: The hydrogel particles that were functionalized with Alexa Fluor 594-conjugated goat IgG (Invitrogen, CA, USA) were imaged with a Leica DMi8 inverted microscope. Using a microscope stage top heater (PE100 Inverted Peltier System, Linkam Scientific, UK), the hydrogel particles were heated sequentially. The temperature was held constant for 5 min at each heating step to allow the hydrogel particles to fully achieve equilibrium. The changes in hydrogel particle diameter and intensity were analyzed using FIJI.[42]

Diffusion Characterization: The hydrogel particles functionalized with antigoat IgG (Invitrogen, CA, USA) were incubated with 5 μg mL^{-1} Alexa Fluor 594-conjugated goat IgG (Invitrogen, CA, USA) for a maximum of 2 h. The binding of the two IgGs was monitored under a Leica DMi8 inverted microscope at a specified time interval. The diffusion coefficients of fluorescein isothiocyanate-dextran molecules within the gel matrices were calculated using the FRAP technique. Thin hydrogel discs containing 0.5 mg mL^{-1} FITC-dextran (20, 70, or 500 k) were fabricated as described above. FRAP images were then taken using an Olympus IX confocal laser scanning microscope using a 40x objective after bleaching, which was performed on a circular region with a laser intensity of 100%.

Droplet Coencaspsulation: The microfluidic coencapsulation device was 50 μm deep and included three inlets for 1) hydrogel particle immunosensors, 2) cell suspension, and 3) carrier oil. Prior to the operation of the device, the channels were treated with 1% trichloro(1H,1H,2H,2H-perfluorooctyl)silane and baked at 120 °C for 10 min. To achieve the close packing of the beads, the hydrogel particles were concentrated by centrifugation, and the pellet was loaded directly into the tubing. The flow of the packed beads was assisted by the prefilled HFE-7500 in the syringe.[37,38] Cells were loaded at $0.5–1.0 \times 10^5$ cells mL^{-1} in 16% Optiprep (Sigma-Aldrich, St. Louis, MO, USA). A magnetic micro stir bar was placed in the cell-loaded syringe so that the cell suspension could be maintained by periodically disturbing the solution with a magnet. The carrier oil was HFE-7500 (3M Novect, Singapore) with 0.15% Pico-Surf 1 (Dolomite, UK). The flow rates used were 30–40 μL h^{-1} for hydrogel particles, 150 μL h^{-1} for cell suspension, and 300 μL h^{-1} for the oil phase, which produced ≈150 μm droplets.

Cell Viability in Droplets: To track the cells, the cells were first incubated with 2 μg mL^{-1} Hoechst 33 342 dye (Life Technologies, Gaithersburg, MD) for 15 min. After washing, the cells were coencapsulated with microgels and 2 μM dead stain ethidium homodimer-1 (Life Technologies, Gaithersburg, MD, USA). Subsequently and after every 24 h, the droplets were imaged using a Leica DMi8 fluorescence inverted microscope. The cell viability was then calculated as $(Cells_{Total}–Cells_{dead})/Cells_{Total}$.

Secreted Protein Detection: The droplets containing cells and immunosensors were collected in HFE7500 containing 2% Pico-Surf 1 and incubated for 24 h in a 37 °C incubator with a 5% CO_2/ 95% air environment. Afterward, the oil phase was carefully exchanged with pure HFE7500 (3M Novect, Singapore) twice before breaking the droplets by centrifugation. The hydrogel particles were resuspended in PBS (Gibco, CA, USA) and washed thoroughly three times with phosphate buffered saline with Tween 20 (PBST) (0.05% Tween 20 (Sigma-Aldrich, St. Louis, MO, USA) in PBS) to remove unbounded proteins. The beads were then probed with reporter antibodies at 1–5 μg mL^{-1} for 30 min before washing three times with PBST. The microbeads were then imaged within an hour.

Supporting Information

Supporting Information is available from the Wiley Online Library or from the author.

Acknowledgements

The authors gratefully acknowledge the funding provided by NMRC OFIRG (R-397-000-289-213), NRF CRP (R-397-000-276-281), NRF EIRP (R-397-000-252-592), NRF BDTA (R-397-000-221-592), and MOE Tier-2 (R-397-000-271-112, R-279-000-501-112, and R-397-000-253-112).

Conflict of Interest

The authors declare no conflict of interest.

Keywords

droplet microfluidics, hydrogel microparticles, immunofluorescence assays, signal enhancements, single cell protein secretions

Received: July 25, 2018
Revised: October 2, 2018
Published online:

[1] M. Kwak, L. Mu, Y. Lu, J. J. Chen, Y. Wu, K. Brower, R. Fan, *Front. Oncol.* **2013**, *3*, 10.
[2] A. A. Cohen, N. Geva-Zatorsky, E. Eden, M. Frenkel-Morgenstern, I. Issaeva, A. Sigal, R. Milo, C. Cohen-Saidon, Y. Liron, Z. Kam, *Science* **2008**, *322*, 1511.
[3] K. Sachs, O. Perez, D. Pe'er, D. A. Lauffenburger, G. P. Nolan, *Science* **2005**, *308*, 523.
[4] J. M. Irish, R. Hovland, P. O. Krutzik, O. D. Perez, Ø. Bruserud, B. T. Gjertsen, G. P. Nolan, *Cell* **2004**, *118*, 217.
[5] T. Jung, U. Schauer, C. Heusser, C. Neumann, C. Rieger, *J. Immunol. Methods* **1993**, *159*, 197.

[6] C. C. Czerkinsky, L. Å. Nilsson, H. Nygren, Ö. Ouchterlony, A. Tarkowski, *J. Immunol. Methods* **1983**, *65*, 109.
[7] S. Palzer, T. Bailey, C. Hartnett, A. Grant, M. Tsang, A. E. Kalyuzhny, *Handbook of ELISPOT*, Springer, Switzerland **2005**, p. 273.
[8] Y. Lu, J. J. Chen, L. Mu, Q. Xue, Y. Wu, P.-H. Wu, J. Li, A. O. Vortmeyer, K. Miller-Jensen, D. Wirtz, *Anal. Chem.* **2013**, *85*, 2548.
[9] K. Miller-Jensen, R. Fan, *Experimental Approaches for the Investigation of Innate Immunity: The Human Innate Immunity Handbook*, World Scientific, Singapore **2016**, p. 41.
[10] M. Rhee, P. Liu, R. J. Meagher, Y. K. Light, A. K. Singh, *Biomicrofluidics* **2014**, *8*, 034112.
[11] E. X. Ng, M. A. Miller, T. Jing, C.-H. Chen, *Biosens. Bioelectron.* **2016**, *81*, 408.
[12] F. Del Ben, M. Turetta, G. Celetti, A. Piruska, M. Bulfoni, D. Cesselli, W. T. Huck, G. Scoles, *Angew. Chem., Int. Ed.* **2016**, *55*, 8581.
[13] L. Mazutis, J. Gilbert, W. L. Ung, D. A. Weitz, A. D. Griffiths, J. A. Heyman, *Nat. Protoc.* **2013**, *8*, 870.
[14] J. Abatemarco, M. F. Sarhan, J. M. Wagner, J.-L. Lin, L. Liu, W. Hassouneh, S.-F. Yuan, H. S. Alper, A. R. Abate, *Nat. Commun.* **2017**, *8*, 332.
[15] K. Eyer, R. C. Doineau, C. E. Castrillon, L. Briseño-Roa, V. Menrath, G. Mottet, P. England, A. Godina, E. Brient-Litzler, C. Nizak, *Nat. Biotechnol.* **2017**, *35*, 977.
[16] V. Chokkalingam, J. Tel, F. Wimmers, X. Liu, S. Semenov, J. Thiele, C. G. Figdor, W. T. Huck, *Lab Chip* **2013**, *13*, 4740.
[17] G. C. Le Goff, R. L. Srinivas, W. A. Hill, P. S. Doyle, *Eur. Polym. J.* **2015**, *72*, 386.
[18] S. Falahati-Pour, A. Lotfi, G. Ahmadian, A. Baghizadeh, *J. Appl. Microbiol.* **2015**, *118*, 976.
[19] E.-P. Lai, Y.-X. Wang, Y. Wei, G. Li, *Polymers* **2016**, *8*, 90.
[20] M. Boulet-Audet, B. Byrne, S. G. Kazarian, *Anal. Chem.* **2014**, *86*, 9786.
[21] K. J. Jeong, A. Panitch, *Biomacromolecules* **2009**, *10*, 1090.
[22] D. C. Appleyard, S. C. Chapin, P. S. Doyle, *Anal. Chem.* **2011**, *83*, 193.
[23] S. Park, H. J. Lee, W.-G. Koh, *Sensors* **2012**, *12*, 8426.
[24] P. Arenkov, A. Kukhtin, A. Gemmell, S. Voloshchuk, V. Chupeeva, A. Mirzabekov, *Anal. Biochem.* **2000**, *278*, 123.
[25] A. G. Lee, C. P. Arena, D. J. Beebe, S. P. Palecek, *Biomacromolecules* **2010**, *11*, 3316.
[26] D. Zubtsov, E. Savvateeva, A. Y. Rubina, S. Pan'kov, E. Konovalova, O. Moiseeva, V. Chechetkin, A. Zasedatelev, *Anal. Biochem.* **2007**, *368*, 205.
[27] T. Si, Y. Wang, W. Wei, P. Lv, G. Ma, Z. Su, *React. Funct. Polym.* **2011**, *71*, 728.
[28] P. Jönsson, M. P. Jonsson, J. O. Tegenfeldt, F. Höök, *Biophys. J.* **2008**, *95*, 5334.
[29] D. C. Pregibon, P. S. Doyle, *Anal. Chem.* **2009**, *81*, 4873.
[30] X.-Z. Zhang, X.-D. Xu, S.-X. Cheng, R.-X. Zhuo, *Soft Matter* **2008**, *4*, 385.
[31] D. Kim, H. Kim, E. Lee, K. S. Jin, J. Yoon, *Chem. Mater.* **2016**, *28*, 8807.
[32] A. Feswick, G. T. Ankley, N. Denslow, L. E. Ellestad, M. Fuzzen, K. M. Jensen, K. Kroll, A. Lister, D. L. MacLatchy, M. E. McMaster, *Environ. Toxicol. Chem.* **2014**, *33*, 847.
[33] A. Graves, D. Henson, M. Padilla, J. Schaeffer, D. Hokey, *J. Immunol.* **2015**, *194*, 207.2.
[34] H. T. Maecker, J. Hassler, J. K. Payne, A. Summers, K. Comatas, M. Ghanayem, M. A. Morse, T. M. Clay, H. K. Lyerly, S. Bhatia, S. A. Ghanekar, *BMC Immunol.* **2008**, *9*, 9.
[35] S. Boulet, M. L. Ndongala, Y. Peretz, M. P. Boisvert, M. R. Boulassel, C. Tremblay, J. P. Routy, R. P. Sekaly, N. F. Bernard, *J. Immunol. Methods* **2007**, *320*, 18.
[36] A. R. Abate, C.-H. Chen, J. J. Agresti, D. A. Weitz, *Lab Chip* **2009**, *9*, 2628.
[37] A. M. Klein, L. Mazutis, I. Akartuna, N. Tallapragada, A. Veres, V. Li, L. Peshkin, D. A. Weitz, M. W. Kirschner, *Cell* **2015**, *161*, 1187.
[38] R. Zilionis, J. Nainys, A. Veres, V. Savova, D. Zemmour, A. M. Klein, L. Mazutis, *Nat. Protoc.* **2017**, *12*, 44.
[39] S. I. Grivennikov, M. Karin, *Ann. Rheum. Dis.* **2011**, *70*, i104.
[40] A. Freund, V. Jolivel, S. Durand, N. Kersual, D. Chalbos, C. Chavey, F. Vignon, G. Lazennec, *Oncogene* **2004**, *23*, 6105.
[41] X. Li, M. Soler, C. Szydzik, K. Khoshmanesh, J. Schmidt, G. Coukos, A. Mitchell, H. Altug, *Small* **2018**, *14*, 1800698.
[42] J. Schindelin, I. Arganda-Carreras, E. Frise, V. Kaynig, M. Longair, T. Pietzsch, S. Preibisch, C. Rueden, S. Saalfeld, B. Schmid, *Nat. Methods* **2012**, *9*, 676.